



TN: 2387645
Pages: 1565-? RIC
Exempt

UBY/UTBG ILL – Lending

Call #: TL 501 .A53x

Location: AUX

Journal Title: AIAA journal.

Volume: 21 Issue: 11

Month/Year: 1983 Pages: 1565-?

Article Author: American Institute of Aeronautics and Astronautics. Pitz, Robert W. and Daily, John W.

Article Title: Combustion in a Turbulent Mixing Layer Formed at a Rearward-Facing Step

ILL Number: 202517047



Lending String:

*UBY,AAU,AD#,AFU,ANC,BMU

Borrower: RIC

Brigham Young University--Idaho

David O. McKay Library---ILL 136

REXBURG, Idaho 83460

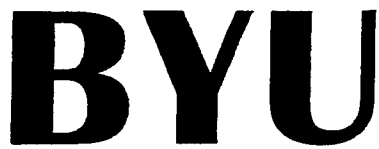
United States

Fax:

Odyssey: illiad.lib.byu.edu

Email: ill@byui.edu

3/18/2020 9:22 AM



**BRIGHAM YOUNG
UNIVERSITY**

Harold B. Lee Library

**Interlibrary Loan
Copy Center**

For Odyssey Receipt Problems:

Phone: 801-422-2953

Fax: 801-422-0471

Email: ill_copy@byu.edu

Odyssey Problem Report

If you have experienced a problem in the delivery of the requested item, please contact us within **Five Business Days** with the following information:

ILL#: _____

Your OCLC Symbol: _____

Date of Receipt: _____

Please specify if:

____ Pages were missing pp. ____ to ____

____ Edges were cut off pp. ____ to ____

____ Illegible copy, resend entire item

____ Wrong article sent

____ Other (explain): _____

NOTICE:

This material may be
protected by copyright
law Title 17 U.S. Code

Combustion in a Turbulent Mixing Layer Formed at a Rearward-Facing Step

Robert W. Pitz* and John W. Daily†
University of California, Berkeley, California

A premixed propane/air flame was stabilized in a turbulent mixing layer formed at a rearward-facing step. The mean and rms averages of the turbulent velocity flowfield were determined by laser velocimetry for both reacting ($\phi=0.57$) and nonreacting flows ($Re=15,000-37,000$ based on step height). The reacting flow was visualized by high-speed schlieren photography. Large-scale structures dominate the reacting mixing layer. The growth of the large-scale structures was tied to the propagation of the flame. The linear growth rate of the reacting mixing layer defined by the mean velocity profiles was unchanged by combustion but the virtual origin moves downstream. The reacting mixing layer boundaries based on the mean velocity profiles were shifted toward the recirculation zone and reattachment lengths were shortened by 30%. The edge of the flame controlled by the large-scale structure development propagated faster into the incoming reactants than the boundary of the mixing layer given by the mean velocity flowfield. Thus, the region of high velocity gradient did not coincide with the region of high reaction and heat transfer.

I. Introduction

METHODS for reducing nitric oxide emissions from aircraft gas turbine combustors have been sought for a number of years,¹ and lean premixed combustion has been found to be particularly effective in this regard.² To study the problem of such a combustion process, we have been experimenting with a model combustor in which the flame is stabilized in a two-dimensional turbulent mixing layer formed at the edge of a rearward-facing step. The rearward-facing step configuration preserves the essential features of premixed combustion with stabilization achieved by recirculation of hot products and at the same time is a simpler configuration to observe and model.

During the initial studies of the combustor,³ the flowfield was found to be dominated by large-scale structures^{4,5} with an ordered pattern previously unreported in combustion flows. The structures were shown to form in the mixing layer trailing the rearward-facing step. The growth of the mixing layer is then controlled by the dynamics of these large eddies which form early in the layer and grow by coalescence with their neighbors and by entrainment of fluid from both sides of the layer. Fine-scale mixing occurs within the structure of the eddies.^{6,7} In the combusting flame, premixed reactants and hot products from the recirculation zone are folded together by eddy entrainment and the burning occurs within the eddies when the components are mixed by diffusion and fine-scale turbulence.

The primary aim of the present work is to assess the effect of combustion on the mean flowfield properties such as mixing layer growth, entrainment rate, and reattachment length. To achieve this goal, the flowfield was visualized with high-speed schlieren photography and quantified by a detailed mapping of the turbulent velocity field by laser Doppler velocimetry (LDV). In a preliminary paper,⁸ the streamwise velocity flowfield was reported for the reacting and nonreacting shear layers at a single entrance Reynolds number. In this paper we report mean and rms averages of

both axial and transverse velocity components measured throughout the mixing layer. The reacting and nonreacting flowfield is studied for three entrance Reynolds numbers ($Re_H=15,000$, 22,000, and 37,000) where the Reynolds number $Re_H=U_0H/\nu$, is based on step height H , average inlet velocity U_0 , and kinematic viscosity ν .

In the following we describe the experimental apparatus and procedure, present the results, and discuss their significance. Finally, the summary and conclusions are given.

II. Experimental Facilities

Two-Dimensional Combustor

The experiments are carried out in the two-dimensional combustor apparatus shown in Fig. 1. The air and propane are combined in three parallel Venturi tubes and mixed in a 1-m-long premix section packed with stainless steel wool for turbulence reduction. The premix section has a cross section 51 mm high and 173 mm wide. The flow converges over the backside of a profiled step with a 2:1 area ratio. The two-dimensional, reattaching shear layer forms at the edge of the 25-mm-high step. The test section is 220 mm long, 173 mm wide, and 51 mm high giving an aspect ratio (channel width to step height) of 6.9. Two 12.7-mm-thick fused quartz windows are mounted on the sides of the test section exposing 13 mm of the step and extending the entire length of the test section. The equivalence ratio can be set to 6% accuracy and inlet flow velocity within 1.3% accuracy. Complete details of the combustor apparatus are given by Pitz and Daily.⁹

Laser Anemometer

The laser anemometer (Fig. 2) consists of a conventional single color, dual beam, forward scatter optical configuration with Bragg cell frequency shifting.⁹ The probe dimensions are given in Fig. 2. The Doppler frequency is analyzed by a period counter which is modified to allow recording of the time between realizations. From data records of 2048 velocity/time pairs, both numerical ($\sum u_i/N$) and time integrated averages ($\langle u(t) dt \rangle/N$) are stored at each point.

Cyclone particle seeders similar to those described by Glass and Kennedy¹⁰ are used to suspend alumina (Al_2O_3) particles into the flow. The alumina particles (0.05 μ nominal diameter) are dried before each experiment to limit agglomeration. The average particle diameter in the airstream is estimated to be 0.2 μ giving a frequency response of 10 kHz for 1% velocity lag.¹¹

Received April 30, 1982; revision received Oct. 12, 1982. Copyright © American Institute of Aeronautics and Astronautics, Inc., 1982. All rights reserved.

*Staff Scientist; presently with General Electric Research and Development Center, Schenectady, New York. Member AIAA.

†Associate Professor, Dept. of Mechanical Engineering. Member AIAA.

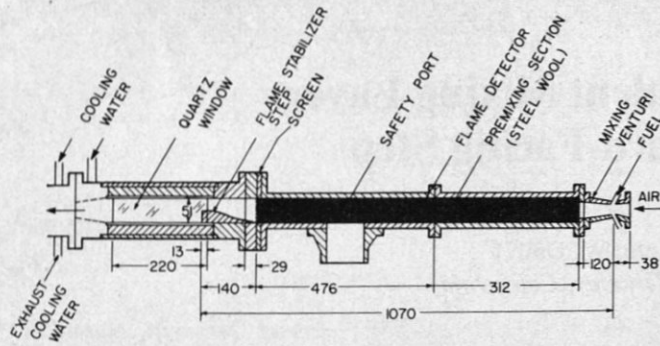


Fig. 1 Cross section of the two-dimensional combustor (all dimensions in mm).

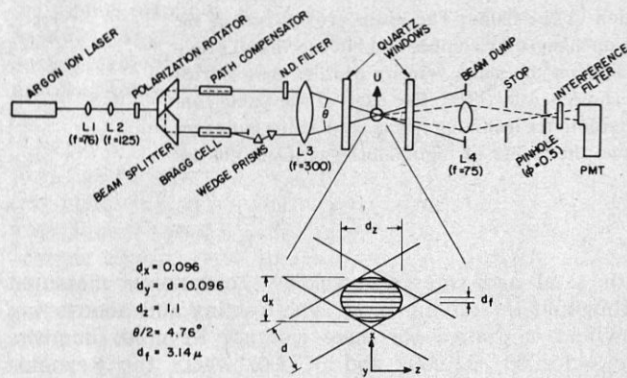


Fig. 2 Two-dimensional combustor LDV optics (all dimensions in mm).

Error Sources

The velocity measurement has an accuracy of 0.4% determined by the counterclock resolution and frequency spacing uncertainty. In combustion systems, velocity biasing, where the particle velocity pdf is different from the actual velocity pdf, can be caused by McLaughlin-Tiederman effects,¹² Bragg cell effects,¹³ and density variations.¹⁴ The velocity biasing due to these effects is circumvented by the use of time integrated averages in the high data rate regions.¹⁵ Interference fringe curvature from misplacement of the beam waist added 0.1% rms turbulence without changing the mean.

Velocity gradient broadening results from velocity gradients in the finite sized focal volume. Errors in the mean velocity estimated according to Kreid¹⁶ are greatest at 0.04% in the boundary layer at separation. At one step downstream, the error is reduced to 0.04%. Spurious turbulence generated by velocity gradients is significant in this flowfield. Gradient broadening of the rms velocity is given by¹¹

$$U_{rmsg} = \left[\frac{1}{4} d_y^2 \left(\frac{\partial u}{\partial y} \right)^2 + \frac{3}{64} d_y^4 \left(\frac{\partial^2 u}{\partial y^2} \right)^2 + \dots \right]^{1/2} \quad (1)$$

where d_y is the probe volume diameter in the y (gradient) direction. The curvature term is small throughout the flowfield but the gradient term accounts for half of the turbulence in the boundary layer at separation and is significant downstream.

All the gradient broadening given by Eq. (1) is removed from the rms velocity data reported here. In the boundary layer the gradient $\partial u / \partial y$ is calculated by a polynomial fit of the mean velocity data. The maximum corrections are $u_{rmsg} / U_0 = 0.04$ to 0.07 for the three entrance Reynolds numbers studied. In the shear layer, $\partial u / \partial y$ is calculated from an error function fit of the mean velocity profiles. The maximum corrections are $u_{rmsg} / U_0 = 0.03$, 0.02, 0.005, for $x/H = 0.5, 1, 2$, respectively.

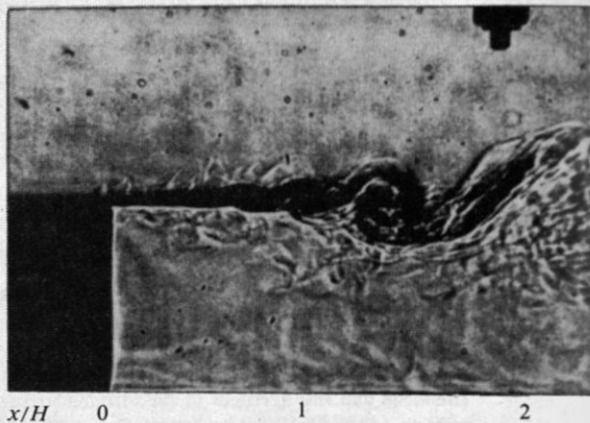


Fig. 3 Schlieren photograph of the initial shear layer for reacting flow ($\phi = 0.57$, $Re_H = 22,000$, $\tau_{exp} = 60 \mu s$).

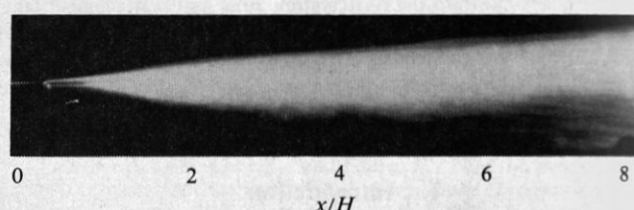


Fig. 4 Long exposure schlieren photograph of the reacting flow ($Re_H = 22,000$, $\phi = 0.57$, $\tau_{exp} = 33 \text{ ms}$).

III. Results

Three Reynolds number conditions ($Re_H = 15,000$, $22,000$, and $37,000$; $H = 25$ mm) were studied for both reacting ($\phi = 0.57$) and nonreacting flows. The Reynolds number limits were determined by the stable burning modes of the combustor. All the inlet conditions were at room temperature and 1 atm pressure. Complete profiles of the mean and rms averages of the u -velocity component were recorded for each flow condition. The reacting flows were visualized with high-speed schlieren photography. Measurements of the v -velocity component were made for one Reynolds number ($Re_H = 22,000$) condition.

Flow Visualization

Schlieren photographs were made for each of the combusting operating conditions. For each condition both short (60 μs) and long time exposures were taken. Figures 3 and 4 show typical short and long exposure records for the $Re_H = 22,000$ case.

Initial Conditions

Entry velocity profiles were obtained for each operating condition. A typical axial velocity profile on centerline is illustrated in Fig. 5. Also shown is the normalized rms velocity profile.

The mean and rms velocities were calculated using numerical ($\Sigma u_i / N$) averages of the data records as the data rates near the wall were too low to make time integrated averages meaningful. To assess the reliability of the laser Doppler anemometer (LDA) results the cold flow measurements were compared with hot wire anemometer measurements. The two agree to within the accuracy of each method. As a second check, the centerline profiles for each condition were integrated to obtain the mass flow rate. The integrated values were within 3% of the flow meter measurements.

The boundary-layer profile at the step was plotted against a Blasius profile for the low Reynolds number case in Fig. 6 and

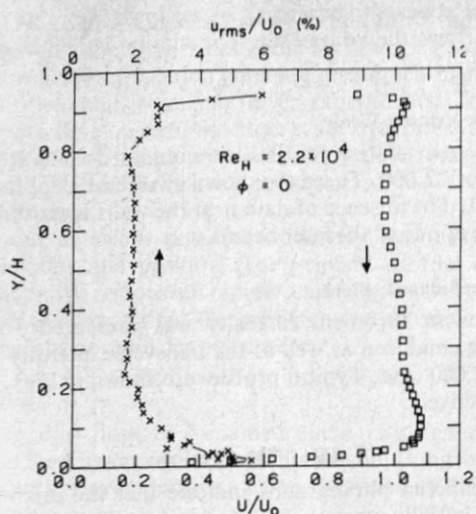
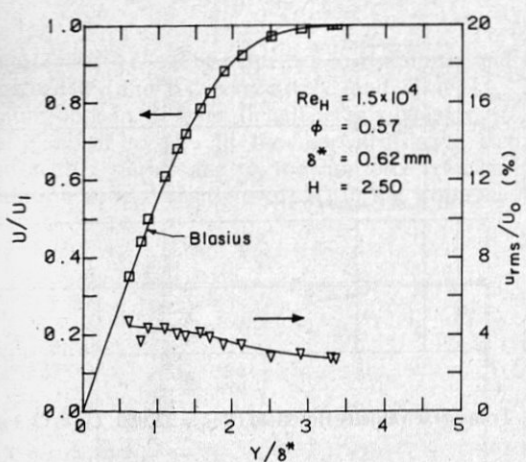
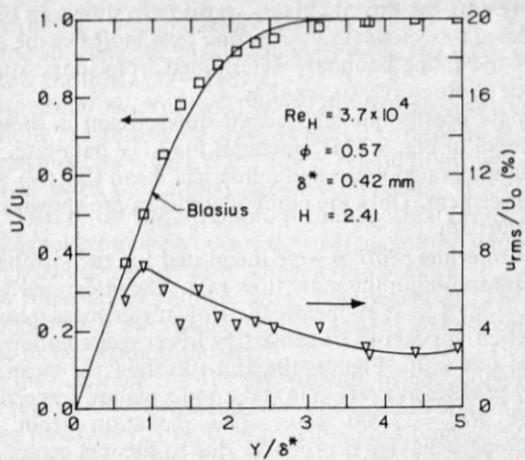
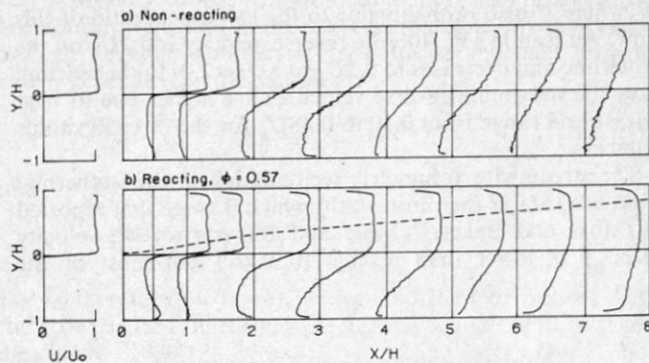
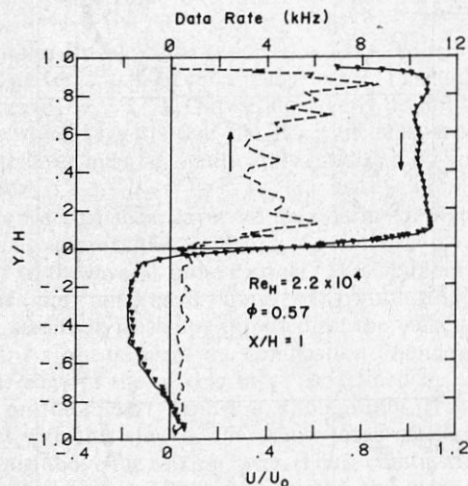
Fig. 5 Entry velocity profile ($x/H = 0, z/H = 0$).Fig. 6 Boundary layer at separation—low Reynolds number ($x/H = 0, z/H = 0$).

Table 1 Entry flow conditions

U_0 , m/s	ϕ	Re_H	Re_θ	δ^* , mm	H_{12}	u_{rms}/U_0	Boundary layer
						Free- stream	
9.1	0.0	15,000	140	0.63	2.58	0.015	0.040
9.1	0.57	15,000	150	0.62	2.50	0.030	0.045
13.3	0.0	22,000	180	0.50	2.46	0.020	0.050
13.3	0.57	22,000	190	0.55	2.48	0.030	0.055
22.2	0.0	37,000	280	0.47	2.42	0.020	0.080
22.2	0.57	37,000	250	0.42	2.41	0.030	0.070

the high Reynolds number case in Fig. 7. For the low Reynolds number flow the mean velocity follows the Blasius profile with a shape factor close to the Blasius value ($H_{12}=2.6$). The turbulence level (corrected for gradient broadening) is high (4%) but flat. The high Reynolds number profile departs more significantly from the Blasius but has a shape factor of 2.4, much larger than the value of 1.3 seen in fully turbulent layers. Also, the turbulence level has increased to 8%.

The boundary-layer parameters are summarized in Table 1 for all the run conditions. The influence of combustion on the state of the boundary layer is minimal. Under all conditions the turbulence levels in the boundary layer are high (4-8%), yet the mean velocity profiles are nearly laminar. [This boundary-layer state is similar to the tripped layer reported by Batt.¹⁷ He used a wire trip producing a boundary layer with

Fig. 7 Boundary layer at separation—high Reynolds number ($x/H = 0, z/H = 0$).Fig. 8 Streamwise velocity flowfield, ($Re_H = 22,000; U_0 = 13.3 \text{ m/s}$; —, flame boundary).Fig. 9 Typical centerline streamwise velocity profile in the shear layer (∇ , time integrated mean velocity; —, numerical mean velocity).

high turbulence levels and a Blasius profile. In our case, imperfections in the profiled step (probably at the leading edge) may have tripped the boundary layer.] The momentum thickness Reynolds numbers are around the critical value of 160 but are well below the transitional value of 390. The boundary layer never becomes fully turbulent and is probably best described as "transitional."

Streamwise Velocity Field

Streamwise velocity profiles were obtained at a number of axial locations for each operating condition. Typical cen-

terline results for the whole test section are shown in Fig. 8. The dashed line shown in the reacting flow indicates the upper edge of the flame boundary determined from long exposure schlieren photographs such as Fig. 4.

A single profile one step height downstream is shown in more detail in Fig. 9 which includes the LDV data rate. Both the time integrated mean and numerical mean ($\Sigma u_i/N$) are in good agreement. Only the numerical means are shown in the rest of the data.

The centerline profiles were integrated for each isothermal condition to obtain the mass flow rate. The integrated values ranged from 8 to 25% below the flow meter measurements. This deficit appears to be caused by lower recirculation rates near the side walls. Figures 10a and 10b show the mean axial velocity profiles at $x/H = 3$ in the y and z planes, respectively, for the $Re_H = 22,000$ case. The deviation from two-dimensional behavior is probably due to the low aspect ratio of the tunnel. Only at aspect ratios greater than 10 have three-dimensional effects been found to be small.¹⁸

The maximum reverse velocity in the nonreacting flow is $0.33U_0$ which is higher than the value ($0.25U_0$) reported elsewhere,¹⁹ also probably due to the low aspect ratio of this flow. As seen in Fig. 10b the reverse velocity is $0.3U_0$ on the centerline and decreases to $0.2U_0$ at $z/H = 2.0$. In the reacting flow the maximum reverse velocities are higher due to heat release and range from 0.39 to $0.48U_0$ for the three Reynolds numbers.

The streamwise volumetric recirculation in the isothermal flow is $0.16U_0H$ (per unit width) which is twice that reported by Moss and Baker.²⁰ Moss and Baker's reverse velocity ($0.2U_0$) is lower than normal ($0.25U_0$) but most of the

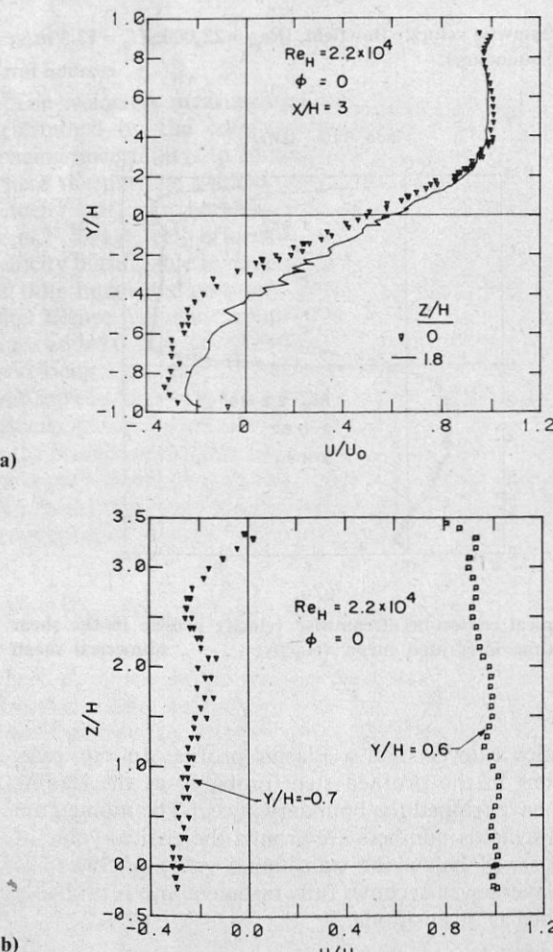


Fig. 10 Two dimensionality of the flowfield. a) Y scan of velocity on and off centerline. b) Z scan of velocity above and below the shear layer ($x/H = 3.0$).

difference appears to be a result of our low aspect ratio. In the reacting flows the volumetric recirculation is higher at $0.16-0.24U_0H$.

Transverse Velocity Field

Transverse velocity profiles were obtained for a Reynolds number of 22,000. These are shown at several axial locations in Fig. 11. The absence of data near the walls is caused by the blockage of one of the laser beams.

Turbulence Intensity Field

Streamwise turbulent intensity was measured for each operating condition as well as the transverse intensity for the $Re_H = 22,000$ case. Typical profiles are shown in Figs. 12 and 13, respectively.

IV. Discussion

The schlieren photographs indicate that the mixing layer develops initially very much like a free layer with zero velocity on one side (half-jet mixing). Unlike half-jet flows, however, the upper velocity, U_1 , does vary slightly with x , the flow is

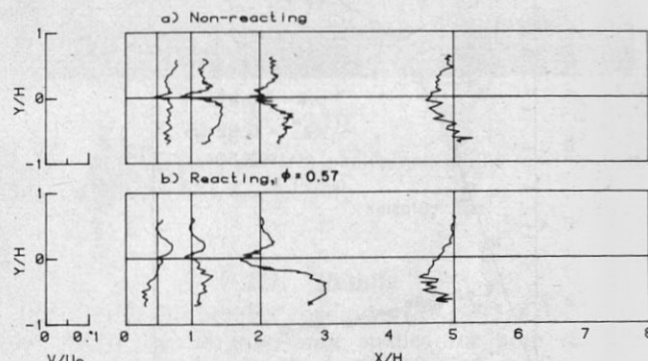


Fig. 11 Transverse velocity flowfield ($Re_H = 22,000$, $U_0 = 13.3 \text{ m/s}$).

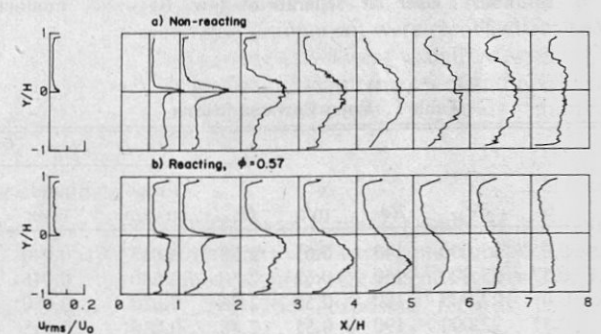


Fig. 12 Streamwise turbulence intensity profiles ($Re_H = 22,000$, $U_0 = 13.3 \text{ m/s}$).

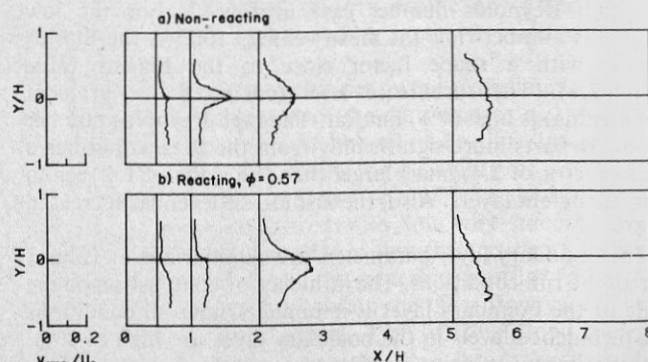


Fig. 13 Transverse turbulence intensity profiles ($Re_H = 22,000$, $U_0 = 13.3 \text{ m/s}$).

not fully two dimensional and, more importantly, the velocity in the recirculation zone is not zero. Turbulence levels in the freestream and recirculation zone are also much higher than in most other half-jet mixing layer experiments. The layer continues to develop until the large-scale structure within the layer approaches the step height and wall effects become important. Also a downward curvature of the developing layer is observed.

From our data it is possible to identify two measures of layer thickness and position. The velocity profiles may be used to identify regions of rapidly changing velocity and to find the mean streamline. The schlieren records may be used to find regions of rapid density change.

Growth Rate

Because our flow is contained there is often no well developed freestream region. For this reason we have chosen to characterize layer thickness using the vorticity thickness, δ_ω , given by

$$\delta_\omega = \Delta U / \left(\frac{\partial u}{\partial y} \right)_{\max} \quad (2)$$

where $\Delta U = U_1 - U_2$. The velocities in the upper and lower streams are U_1 and U_2 , respectively, and $\partial U / \partial y|_{\max}$ is the maximum slope in the layer. In half-jet mixing layers ($U_2 = 0$), ΔU is identical to U_1 . In the rearward-facing step configuration, U_2 varies due to the nonzero velocity in the recirculation zone. Variations of ΔU in the isothermal flow

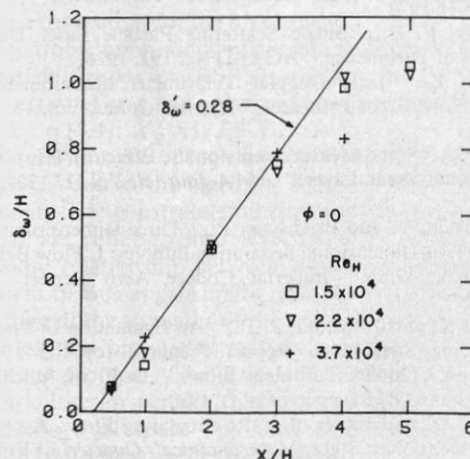


Fig. 14 Vorticity thickness of the nonreacting shear layers (— linear fit of $Re_H = 37,000$).

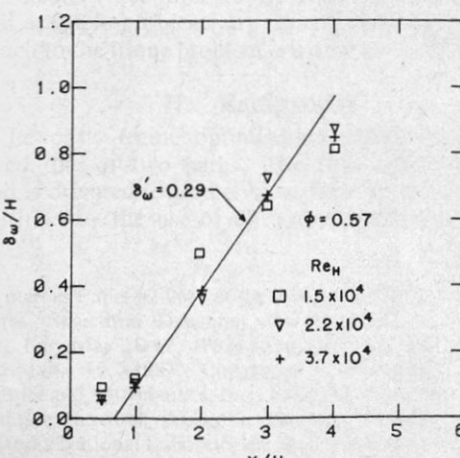


Fig. 15 Vorticity thickness of the reacting shear layers (— linear fit of $Re_H = 37,000$).

are 1.1 to $1.3U_1$ and in the reacting flow 1.1 to $1.5U_1$. Here δ_ω is estimated using the maximum velocity in the recirculation zone near the mixing layer edge.

The velocity thicknesses for the isothermal and reacting conditions are shown in Figs. 14 and 15, respectively. The isothermal curves have a fairly linear region of growth which rolls over when wall effects become important. If a straight line is fitted to the linear region, then the virtual origin for all three Reynolds numbers occurs downstream of the step.

The reacting curves also show a fairly linear region of growth followed by rollover as δ_ω approaches H . The main difference is that the virtual origin is shifted downstream and that the linear region is shorter.

One may characterize the growth rate by the slope of the linear region, δ'_ω . Estimates for both our isothermal and reacting flows vary from 0.26 to 0.29 and are practically the same for the isothermal and reacting cases at each Reynolds number. These growth rates are much higher than those reported previously. Only the growth rates of tripped half-jet mixing layers¹⁷ approach this value ($\delta'_\omega = 0.23$).

The excess growth of the isothermal layer may be traced to the nonzero velocities in the recirculation zone. Mixing layers at high Reynolds numbers are self-similar and their growth rate is dependent on the parameters

$$s = \rho_2 / \rho_1 \quad (3)$$

and

$$\lambda = (U_1 - U_2) / (U_1 + U_2) \quad (4)$$

For isothermal flow ($s = 1$), Brown and Roshko⁴ report that the growth rate is linearly dependent on λ and the fit to their data gives $\delta'_\omega = 0.18\lambda$. For half-jet mixing layers ($\lambda = 1$) the growth rate would be 0.18. In rearward-facing step flows the negative velocity in the recirculation zone causes the value of λ to vary between 1.2 and 2.0 in the mixing layer region of the flow. An average value of 1.6 could account for our high rates.

Brown and Roshko also reported a 25% reduction in the growth rate for a half-jet mixing layer ($\lambda = 1$) at high density differences ($\rho_2 / \rho_1 = 1/7$). Our results clearly do not show this behavior which suggests that the effect of density difference across the layer may be significantly modified by volumetric expansion.

For the reacting shear layer we may define an appropriate thickness using the schlieren record. As seen in Fig. 4, the top boundary of the layer is quite distinct. This boundary, which represents the uppermost limit of combustion (within schlieren sensitivity), is superimposed on the velocity record of Fig. 8. As can be seen, the combustion boundary is well above the edge of the mixing layer as defined by the mean velocity profile. Short exposure photographs (Fig. 6) are consistent with this view as they show large-scale structures propagating above the mixing layer. Thus, combustion is not confined to the mixing layer defined by the mean velocity flowfield.

Entrainment

From Fig. 8 it is evident that the reacting shear layer defined by the velocity profiles undergoes a shift downstream into the recirculation zone. The upper stream velocity $U_1(x)$

Table 2 Reattachment lengths

Re_H	x_R/H	
	$\phi = 0$	$\phi = 0.57$
15,000	6.5	4.3
22,000	7.0	4.5
37,000	6.8	5.3

is nearly identical for both the reacting and nonreacting flows. Thus, the mass rate of entrainment of fluid from the upper stream into the mixing layer is reduced for the reacting flow.

Reattachment

The reattachment length is defined as the point in the separation region where there is no net flow reversal. It can be estimated from the velocity flowfield plots. Reattachment lengths for each operating condition are summarized in Table 2. (Velocity profiles are taken in increments of H near the reattachment point making the values accurate to $\pm 0.5H$.) The reattachment lengths for the reacting layers are reduced by 20-30%.

V. Summary and Conclusions

The velocity flowfield of a mixing layer formed at the edge of a rearward-facing step has been studied under both reacting and nonreacting conditions to assess the effect of combustion. The growth rate given by the vorticity thickness is unchanged. The mixing layer defined by the velocity field is shifted by reaction toward the recirculation zone and the reattachment lengths are shortened by 30%. This also reduces the mass rate of entrainment of inviscid fluid into the mixing layer. As seen by schlieren visualization, the reaction takes place largely in the two-dimensional eddies which are not confined to the velocity gradient region. The edge of the flame defined by the reacting eddies spreads faster into the inviscid premixed reactants than the mixing layer defined by the mean velocity. In the reacting mixing layer, the region of high velocity gradient does not coincide with the region of high reaction and heat transfer.

Acknowledgments

This work was supported by National Science Foundation Grant ENG 77-02019 and NASA Grant NSG-3227. The authors wish to thank research scientist Gary Hubbard and graduate student Jay Keller for their support and helpful conversations. We are indebted to D. Jensen, K. Hom, and V. Locke for their technical assistance.

References

- ¹Jones, R. E., Diehl, L. A., Petrasch, D. A., and Grobman, J., "Results and Status of the NASA Aircraft Engine Emission Reduction Technology Programs," NASA TM-79009, Oct. 1978.
- ²Lefebvre, A. H., ed., "Lean Premixed/Prevaporized Combustion," NASA CP-2016, Jan. 1977.
- ³Ganji, A. R. and Sawyer, R. F., "Turbulence, Combustion, Pollutant, and Stability Characterization of a Premixed, Step Combustor," NASA Rept. 3230, 1980.

⁴Brown, G. L. and Roshko, A., "On Density Effects and Large Structure in Turbulent Mixing Layers," *Journal of Fluid Mechanics*, Vol. 64, 1974, pp. 775-816.

⁵Winant, C. D. and Browand, F. K., "Vortex Pairing: The Mechanism of Turbulent Mixing-Layer Growth at Moderate Reynolds Number," *Journal of Fluid Mechanics*, Vol. 63, 1974, pp. 237-255.

⁶Konrad, J. H., "An Experimental Investigation of Mixing in Two Dimensional Shear Flows with Applications to Diffusion Limited Chemical Reactions," SQUID Rept. CIT-8-PU, 1976.

⁷Breidenthal, R. E., "A Chemical Reacting Turbulent Shear Layer," Ph.D. Thesis, California Institute of Technology, 1978.

⁸Pitz, R. W. and Daily, J. W., "Experimental Studies of Combustion in a Two-Dimensional Free Shear Layer," paper presented at the 2nd Symposium on Turbulent Shear Flows, Imperial College, London, July 1979.

⁹Pitz, R. W., "An Experimental Study of Combustion: The Turbulent Structure of a Reacting Shear Layer Formed at a Rearward-Facing Step," Ph.D. Thesis, University of California, Berkeley, 1981; also, Pitz, R. W. and Daily, J. W., NASA CR-165427, 1981.

¹⁰Glass, M. and Kennedy, I. M., "An Improved Seeding Method for High Temperature Laser Doppler Velocimetry," *Combustion and Flame*, Vol. 29, 1977, pp. 333-335.

¹¹Durst, F., Melling, A., and Whitelaw, J. H., *Principles and Practice of Laser-Doppler Anemometry*, Academic Press, New York, 1976.

¹²McLaughlin, D. K. and Tiederman, W. G., "Biassing Correction for Individual Realization of Laser Anemometer Measurements in Turbulent Flows," *The Physics of Fluids*, Vol. 16, 1973, pp. 2082-2088.

¹³Meyers, J. F. and Clemons, J. I. Jr., "Processing Laser Velocimeter High-Speed Burst Counter Data," *Laser Velocimetry and Particle Sizing*, edited by H. D. Thompson and W. H. Stevenson, Hemisphere Publishing Co., N.Y., 1979.

¹⁴Self, S. A. and Whitelaw, J. H., "Laser Anemometry for Combustion Research," *Combustion Science and Technology*, Vol. 13, 1976, pp. 171-197.

¹⁵Dimotakis, P. E., "Single Scattering Particle Laser Doppler Measurements of Turbulence," AGARD No. 193, 1976.

¹⁶Kreid, D. K., "Laser-Doppler Velocimeter Measurements in Nonuniform Flow: Error Estimates," *Applied Optics*, Vol. 13, 1974, pp. 1872-1881.

¹⁷Batt, R. G., "Some Measurements on the Effect of Tripping the Two-Dimensional Shear Layer," *AIAA Journal*, Vol. 13, 1975, pp. 245-247.

¹⁸de Brederode, V. and Bradshaw, P., "Three-Dimensional Flow in Nominally Two-Dimensional Separation Bubbles: I. Flow Behind a Rearward Facing Step," Imperial College Aero Report 72-19, London, 1972.

¹⁹Eaton, J. K. and Johnston, J. P., "An Evaluation of Data for Backward-Facing Step Flow: Report Prepared for the 1980/81 Conferences on Complex Turbulent Flows," Dept. of Mechanical Engineering, Stanford University, Calif., 1980.

²⁰Moss, W. D. and Baker, S., "Re-circulating Flows Associated with Two-Dimensional Steps," *Aeronautical Quarterly*, Vol. 31, 1980, pp. 151-172.